

STATIC BEHAVIOR OF FGM CYLINDRICAL PANEL WITH POROSITIES IN HYGRO-THERMAL ENVIRONMENT

Chu Thanh Binh^{1,2}, Nguyen Van Long^{1,2*}, Tran Minh Tu^{1,2}

¹Hanoi University of Civil Engineering, Hanoi, Vietnam

²Frontier research group of Mechanics of Advanced Materials and Structures (MAMS)-HUCE, Hanoi, Vietnam

*Corresponding author: longnv@huce.edu.vn

(Received: September 04, 2024; Revised: September 26, 2024; Accepted: October 15, 2024)

DOI: 10.31130/ud-jst.2024.533E

Abstract - In this study, the deflection and stress field of perfect and imperfect (with and without porosities) functionally graded (FG) cylindrical panels are determined following the first-order shear deformation theory (FSDT). The panel rested on the two-parameter elastic foundation (Pasternak foundation) under pressure loads and worked in a hygro-thermal environment. Navier's solution has been used for simply supported cylindrical panels to analyze the effects of porosity, geometrical and foundation parameters, as well as temperature and humidity on deflection and stress field. The validated examples demonstrate the reliability of the solution and the self-written Matlab program. Numerical investigations show a significant hygro-thermal effect on the static response of the FG panel.

Key words - Cylindrical panel; static analysis; functionally graded material; porosity; first-order shear deformation theory.

1. Introduction

As a part of advanced materials, functionally graded materials (FGMs) have attracted the attention of both domestic and international scientists since their first appearance in the late 18th century. Due to their superior mechanical properties, FGMs are the ideal selection for manufacturing high-performance structures. These structures had potential applications in adverse environmental conditions such as fuel combustion chambers, thermal shields for aircraft, plasma-facing surfaces in nuclear reactors, and conduits in heat exchange equipment [1]. Cylindrical panel components are widely used in aircraft fuselages or nose sections of flying objects which typically endure high temperatures during operation. These structures are inhomogeneous, so it is crucial to study their behavior under normal working conditions [2-4], while behavior in high-temperature environments [5-7] poses a significant challenge for scientists.

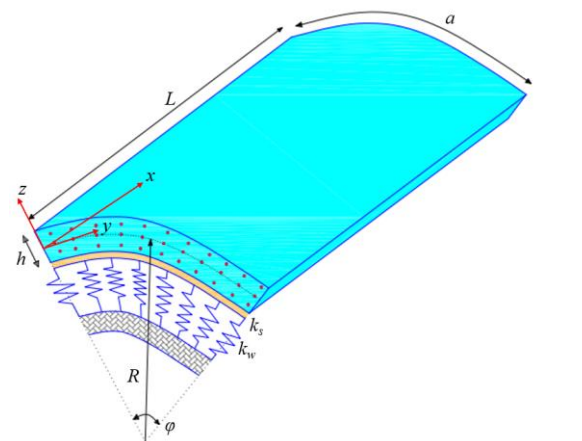
During the manufacturing process of FGMs, microscopic voids may appear within the material structure, especially when using the non-pressure sintering technique [8]. The presence of these micro-voids significantly reduces the load-bearing capacity of FGMs with porosities (FGMPo) [8, 9]. Studies on the mechanical behavior of imperfect FGM plates (with porosities) and perfect cylindrical panels in thermal environments have been published by several authors. However, no publications on the static behavior of FGM cylindrical panels, taking into account the hygrothermal effects, were found in open sources. This is an issue that cannot be ignored for structures operating in environments with high humidity and simultaneously under high-temperature conditions.

Following the previous results of bending and vibration analysis of FGMPo panels [10, 11], this study, based on First-Order Shear Deformation Theory (FSDT), the deflection and stress fields in FGMPo cylindrical panels with even and uneven porosity distributions in hygrothermal environment are determined. The temperature and moisture fields are assumed to be either constant or linearly varying across the panel thickness. The Navier solution is employed to provide explicit form of displacement and stress fields of simply supported FGMPo cylindrical panels. After verifying the solution and a handmade Matlab program as well, the impact of porosity, temperature, moisture, foundation parameters, and geometric dimensions on the static behavior of FGMPo cylindrical panels is evaluated through numerical investigations.

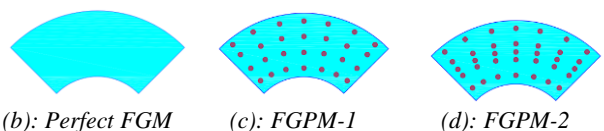
2. Theoretical Approach

2.1. Porous FGMPo Cylindrical Panel

Consider an FGMPo cylindrical panel (Figure 1), with thickness h , length L , and circumferential length a . The panel is placed on an elastic foundation with two stiffness coefficients: k_w is the Winkler stiffness coefficient; k_s is the shear stiffness coefficient.



(a): FGMPo cylindrical panel resting on elastic foundation



(b): Perfect FGM

(c): FGPM-1

(d): FGPM-2

Figure 1. FGMPo cylindrical panel on an elastic foundation and three types of porosity distributions

The FGMPo material consists of two constituent phases: ceramic and metal; the effective properties P_{eff} are assumed to vary smoothly according to a power law (P-FGM) along the panel thickness. The top surface is ceramic-rich, while the bottom surface is metal-rich.

In terms of the imperfect FGMPo panel, pores develop along the shell thickness due to manufacturing defects. Two types of porosity distributions are considered: even porosity distribution (FGMPo - 1) and uneven porosity distribution (FGMPo - 2), which are concentrated on the mid-surface of the shell and decrease linearly to zero at the top and bottom surfaces. Especially, a perfect FGM material (without microvoids) can also be obtained. The material properties of FGMPo include Young's modulus E , Poisson's ratio ν , thermal expansion coefficient α and moisture concentration expansion coefficient β as follows [12, 13]:

$$P_{eff}(z) = P_m + P_{cm} \left(\frac{z}{h} + \frac{1}{2} \right)^p - \frac{\xi}{2} (P_c + P_m) \psi(z) \quad (1)$$

where: $P_{cm} = P_c - P_m$, p is the volume fraction exponent ($p \geq 0$); ξ is the porosity coefficient; $\psi(z)$ is the function dependent on the porosity distribution:

$$\psi(z) = \begin{cases} 0 & \text{(FGM)} \\ 1 & \text{(FGMPo - 1)} \\ (1 - 2|z|/h) & \text{(FGMPo - 2)} \end{cases} \quad (2)$$

2.2. Static Equilibrium Equations

According to FSDT theory, the displacement field of the cylindrical panel can be expressed as [14]:

$$\mathbf{u} = \begin{Bmatrix} u \\ v \\ w \end{Bmatrix} = \begin{Bmatrix} u_0(x, y) \\ v_0(x, y) \\ w_0(x, y) \end{Bmatrix} + z \begin{Bmatrix} \theta_x(x, y) \\ \theta_y(x, y) \\ 0 \end{Bmatrix} = \mathbf{u}_0 + z\boldsymbol{\theta} \quad (3)$$

where: u_0, v_0, w_0 are the displacements on the mid-surface along the axis x, y, z ; θ_x, θ_y are the rotation angles of the mid-surface normal around the y -axis and x -axis, respectively.

The strain field can be expressed in the form:

$$\boldsymbol{\varepsilon} = \begin{Bmatrix} \varepsilon_x \\ \varepsilon_y \\ \gamma_{xy} \end{Bmatrix} = \begin{Bmatrix} u_{0,x} \\ v_{0,y} + \frac{w_0}{R} \\ u_{0,y} + v_{0,x} \end{Bmatrix} + z \begin{Bmatrix} \theta_{x,x} \\ \theta_{y,y} \\ \theta_{x,y} + \theta_{y,x} \end{Bmatrix} \quad (4)$$

$$= \boldsymbol{\varepsilon}_0 + z\boldsymbol{\kappa};$$

$$\boldsymbol{\gamma} = \begin{Bmatrix} \gamma_{xz} \\ \gamma_{yz} \end{Bmatrix} = \begin{Bmatrix} w_{0,x} + \theta_x \\ w_{0,y} + \theta_y \end{Bmatrix} = \boldsymbol{\gamma}_0$$

The stress - strain relation is written as follows:

$$\boldsymbol{\sigma} = \begin{Bmatrix} \sigma_x \\ \sigma_y \\ \sigma_{xy} \end{Bmatrix} = \begin{bmatrix} Q_{11} & Q_{12} & 0 \\ Q_{12} & Q_{22} & 0 \\ 0 & 0 & Q_{66} \end{bmatrix} \begin{Bmatrix} \varepsilon_x - \alpha\Delta T - \beta\Delta C \\ \varepsilon_y - \alpha\Delta T - \beta\Delta C \\ \gamma_{xy} \end{Bmatrix}; \quad (5)$$

$$\boldsymbol{\tau} = \begin{Bmatrix} \sigma_{xz} \\ \sigma_{yz} \end{Bmatrix} = \begin{bmatrix} G(z) & 0 \\ 0 & G(z) \end{bmatrix} \begin{Bmatrix} \gamma_{xz} \\ \gamma_{yz} \end{Bmatrix}$$

$$\text{where: } Q_{11} = Q_{22} = \frac{E(z)}{1 - \nu^2(z)}, Q_{12} = \frac{E(z)\nu(z)}{1 - \nu^2(z)},$$

$$Q_{66} = G(z) = \frac{E(z)}{2[1 + \nu(z)]};$$

$$\Delta T = T - T_0, \Delta C = C - C_0,$$

T_0, C_0 are the reference temperature and moisture concentration, respectively.

The stress resultants of the panel are defined as follows:

$$(\mathbf{N}, \mathbf{M}) = \left(\begin{Bmatrix} N_x \\ N_y \\ N_{xy} \end{Bmatrix}, \begin{Bmatrix} M_x \\ M_y \\ M_{xy} \end{Bmatrix} \right) = \int_{-h/2}^{h/2} \begin{Bmatrix} \sigma_x \\ \sigma_y \\ \sigma_{xy} \end{Bmatrix} (1, z) dz; \quad (6)$$

$$\mathbf{Q} = \begin{Bmatrix} Q_x \\ Q_y \end{Bmatrix} = k_c \int_{-h/2}^{h/2} \begin{Bmatrix} \sigma_{xz} \\ \sigma_{yz} \end{Bmatrix} dz$$

where k_c is the shear correction factor.

By substituting relation (5) into (6), the stress resultants can be rewritten in the following form:

$$\mathbf{N} = \mathbf{A}\boldsymbol{\varepsilon}_0 + \mathbf{B}\boldsymbol{\kappa} - \hat{\mathbf{N}}^T - \hat{\mathbf{N}}^C; \quad (7)$$

$$\mathbf{M} = \mathbf{B}\boldsymbol{\varepsilon}_0 + \mathbf{D}\boldsymbol{\kappa} - \hat{\mathbf{M}}^T - \hat{\mathbf{M}}^C; \quad \mathbf{Q} = \mathbf{A}^s \boldsymbol{\gamma}_0$$

$$\text{where: } (A_{ij}, B_{ij}, D_{ij}) = \int_{-h/2}^{h/2} Q_{ij} (1, z, z^2) dz;$$

$$\mathbf{A}^s = k_c \int_{-h/2}^{h/2} G(z) dz; \quad \hat{\mathbf{N}}^T = \begin{Bmatrix} \hat{N}^T \\ \hat{N}^T \\ 0 \end{Bmatrix}; \quad \hat{\mathbf{M}}^T = \begin{Bmatrix} \hat{M}^T \\ \hat{M}^T \\ 0 \end{Bmatrix};$$

$$\hat{\mathbf{N}}^C = \begin{Bmatrix} \hat{N}^C \\ \hat{N}^C \\ 0 \end{Bmatrix}; \quad \hat{\mathbf{M}}^C = \begin{Bmatrix} \hat{M}^C \\ \hat{M}^C \\ 0 \end{Bmatrix};$$

$$(\hat{N}^T, \hat{M}^T) = \int_{-h/2}^{h/2} \frac{E(z)}{[1 - \nu(z)]} \alpha(z) \Delta T (1, z) dz;$$

$$(\hat{N}^C, \hat{M}^C) = \int_{-h/2}^{h/2} \frac{E(z)}{[1 - \nu(z)]} \beta(z) \Delta C (1, z) dz.$$

Static equilibrium equations of cylindrical panel resting on elastic foundation, under transverse load q can be given in the form [14]:

$$N_{x,x} + N_{xy,y} = 0; \quad N_{xy,x} + N_{y,y} = 0;$$

$$Q_{x,x} + Q_{y,y} - \frac{N_y}{R} - f_e + q = 0; \quad (8)$$

$$M_{x,x} + M_{xy,y} - Q_x = 0; \quad M_{xy,x} + M_{y,y} - Q_y = 0$$

The Pasternak's substrate reaction f_e is defined [15, 16]:

$$f_e = -k_w w_0 + k_s \nabla^2 w_0 \quad (9)$$

Substituting Eq. (7) into (8), equilibrium equations in terms of the displacement components are obtained as follows:

$$\begin{aligned} & A_{11}u_{0,xx} + A_{66}u_{0,yy} + (A_{12} + A_{66})v_{0,xy} + \frac{A_{12}}{R}w_{0,x} \\ & + B_{11}\theta_{x,xx} + B_{66}\theta_{x,yy} + (B_{12} + B_{66})\theta_{y,xy} \\ & = \hat{N}_{,x}^T + \hat{N}_{,x}^C; \\ & (A_{12} + A_{66})u_{0,xy} + A_{22}v_{0,yy} + A_{66}v_{0,xx} + \frac{A_{22}}{R}w_{0,y} \\ & + (B_{12} + B_{66})\theta_{x,xy} + B_{22}\theta_{y,yy} + B_{66}\theta_{y,xx} \\ & = N_{,y}^T + N_{,y}^C; \\ & -\frac{A_{12}}{R}u_{0,x} - \frac{A_{22}}{R}v_{0,y} - \left(\frac{A_{22}}{R^2} + k_w\right)w_0 \\ & + (A^s + k_s)\nabla^2 w_0 + \left(A^s - \frac{B_{12}}{R}\right)\theta_{x,x} \\ & + \left(A^s - \frac{B_{22}}{R}\right)\theta_{y,y} + q + \frac{1}{R}(\hat{N}^T + \hat{N}^C) = 0; \\ & B_{11}u_{0,xx} + B_{66}u_{0,yy} + (B_{12} + B_{66})v_{0,xy} \\ & + \left(\frac{B_{12}}{R} - A^s\right)w_{0,x} + D_{11}\theta_{x,xx} + D_{66}\theta_{x,yy} \\ & + (D_{12} + D_{66})\theta_{y,xy} - A^s\theta_x = \hat{M}_{,x}^T + \hat{M}_{,x}^C; \\ & (B_{12} + B_{66})u_{0,xy} + B_{66}v_{0,xx} + B_{22}v_{0,yy} + \left(\frac{B_{22}}{R} - A^s\right)w_{0,y} \\ & + (D_{12} + D_{66})\theta_{x,xy} + D_{66}\theta_{y,xx} + D_{22}\theta_{y,yy} - A^s\theta_y \\ & = \hat{M}_{,y}^T + \hat{M}_{,y}^C \end{aligned} \quad (10)$$

2.3. Navier solution

For the simply supported (SS) cylindrical panel, the boundary condition expressions are as follows:

$$\begin{aligned} & \text{At edge } x = 0 \text{ and } x = L: \\ & v_0 = w_0 = \theta_y = N_x = M_x = 0; \\ & \text{At edge } y = 0 \text{ and } y = a: \\ & u_0 = w_0 = \theta_x = N_y = M_y = 0 \end{aligned} \quad (11)$$

Based on Navier's technique the expansions of displacements are assumed to be satisfied the SS boundary conditions:

$$\begin{aligned} (u_0, \theta_x) &= \sum_{m=1}^{\infty} \sum_{n=1}^{\infty} (U_{mn}, X_{mn}) \cos rx \sin sy; \\ (v_0, \theta_y) &= \sum_{m=1}^{\infty} \sum_{n=1}^{\infty} (V_{mn}, Y_{mn}) \sin rx \cos sy; \\ w_0 &= \sum_{m=1}^{\infty} \sum_{n=1}^{\infty} W_{mn} \sin rx \sin sy \end{aligned} \quad (12)$$

where: $m, n = 1, 2, 3, \dots$; $U_{mn}, V_{mn}, W_{mn}, X_{mn}, Y_{mn}$ are unknown coefficients; $r = \frac{m\pi}{L}, s = \frac{n\pi}{a}$.

The transverse load q and hygro-thermal forces are also expanded in double-Fourier series as:

$$\begin{Bmatrix} q \\ \hat{N}^T \\ \hat{N}^C \\ \hat{M}^T \\ \hat{M}^C \end{Bmatrix} = \sum_{m=1}^{\infty} \sum_{n=1}^{\infty} \begin{Bmatrix} q_{mn} \\ \hat{N}_{mn}^T \\ \hat{N}_{mn}^C \\ \hat{M}_{mn}^T \\ \hat{M}_{mn}^C \end{Bmatrix} \sin rx \sin sy \quad (13)$$

The transverse load and hygro-thermal force coefficients are given below:

$$\begin{Bmatrix} q_{mn} \\ \hat{N}_{mn}^T \\ \hat{N}_{mn}^C \\ \hat{M}_{mn}^T \\ \hat{M}_{mn}^C \end{Bmatrix} = \frac{4}{La} \int_0^L \int_0^a \begin{Bmatrix} q \\ \hat{N}^T \\ \hat{N}^C \\ \hat{M}^T \\ \hat{M}^C \end{Bmatrix} \sin rx \sin sy dx dy \quad (14)$$

Substituting Eqs. (12) - (13) into (10) to get the following algebraic $\forall m, n$:

$$[K] \begin{Bmatrix} U_{mn} \\ V_{mn} \\ W_{mn} \\ X_{mn} \\ Y_{mn} \end{Bmatrix} = \begin{Bmatrix} 0 \\ 0 \\ q_{mn} \\ 0 \\ 0 \end{Bmatrix} - \begin{Bmatrix} r\hat{N}_{mn}^T \\ s\hat{N}_{mn}^T \\ 0 \\ r\hat{M}_{mn}^T \\ s\hat{M}_{mn}^T \end{Bmatrix} - \begin{Bmatrix} r\hat{N}_{mn}^C \\ s\hat{N}_{mn}^C \\ 0 \\ r\hat{M}_{mn}^C \\ s\hat{M}_{mn}^C \end{Bmatrix} \quad (15)$$

where stiffness matrix $[K]$ is symmetric; the remaining

non-zero coefficients include: $k_{11} = A_{11}r^2 + A_{66}s^2$;

$$k_{12} = (A_{12} + A_{66})rs; \quad k_{13} = -\frac{A_{12}}{R}r; \quad k_{14} = B_{11}r^2 + B_{66}s^2;$$

$$k_{15} = k_{24} = (B_{12} + B_{66})rs; \quad k_{22} = A_{66}r^2 + A_{22}s^2;$$

$$k_{23} = -\frac{A_{22}}{R}s; \quad k_{25} = B_{66}r^2 + B_{11}s^2;$$

$$k_{33} = \frac{A_{22}}{R^2} + k_w + (A^s + k_s)(r^2 + s^2); \quad k_{34} = \left(A^s - \frac{B_{12}}{R}\right)r;$$

$$k_{35} = \left(A^s - \frac{B_{22}}{R}\right)s; \quad k_{44} = D_{11}r^2 + D_{66}s^2 + A^s;$$

$$k_{45} = (D_{12} + D_{66})rs; \quad k_{55} = D_{66}r^2 + D_{11}s^2 + A^s.$$

3. Numerical Studies

Based on proposed Navier solution, a Matlab code is written to analyze numerical studies with the shear correction factor as $k_c = 5/6$. FGMPo cylindrical panel (Al/Al₂O₃) has the following mechanical properties [17]:

- Al (aluminum): $E_m = 70$ GPa, $\alpha_m = 23 \times 10^{-6}$ (1/°C),

$$\beta_m = 0.44, \nu_m = 0.3.$$

- Al₂O₃ (alumina): $E_c = 380$ GPa, $\alpha_c = 7 \times 10^{-6}$ (1/°C),
 $\beta_c = 0.001, \nu_c = 0.3.$

The non-dimensional parameters are defined as follows [18]:

$$\begin{aligned} w^*(x) &= \frac{10E_c h^3}{qa^4} \times w_0 \left(x, \frac{a}{2} \right), \\ \sigma_x^*(z) &= \frac{h}{qL} \times \sigma_x \left(\frac{L}{2}, \frac{a}{2}, z \right), \\ \bar{w} &= \frac{10E_c h^3}{qa^4} \times w_0 \left(\frac{L}{2}, \frac{a}{2} \right), \bar{\sigma}_x = \frac{h}{qL} \times \sigma_x \left(\frac{L}{2}, \frac{a}{2}, \frac{h}{2} \right) \\ K_0 &= \frac{k_w L^4}{D_m}, J_0 = \frac{k_s L^2}{D_m}, D_m = \frac{E_m h^3}{12(1-\nu_m^2)} \end{aligned} \quad (16)$$

There are two cases of studies obtained to confirm the solution reliability: (i) Verification of the deflection of the FGM cylindrical panel under mechanical load; (ii) Verification of the deflection of the FGM plate subjected to mechanical-thermal-moisture loads.

Table 1 presents non-dimensional deflection

$$\tilde{w} = \frac{1}{h} \times w_0 \left(\frac{a}{2}, \frac{b}{2} \right)$$

of FGMPo cylindrical panel (Al/ZrO₂) under uniform transverse load: $q = 10^6$ Pa, $h = 0.01$ m, $L = a = 0.2$ m. The results are compared to solutions given by Sander and Zhao et al. [7].

Table 1. Non-dimensional deflection \tilde{w} FGMPo cylindrical panel with various p

p	Zhao and cs. [7]	Present	Differences (%)
0	0.04267	0.04264	0.07
0.5	0.05425	0.05421	0.07
1	0.06072	0.06067	0.08
2	0.06658	0.06652	0.09
5	0.07235	0.07229	0.08

Table 2. Non-dimensional deflection \hat{w} of FGM plate with various foundation coefficients and geometrical parameter a/h

Sources	$a/h = 10$	$a/h = 20$	$a/h = 50$
$K_0 = 0, J_0 = 0$			
Zidi et al. [19]	1.79156	0.71642	0.41516
Present	1.79221	0.71637	0.41514
Difference(%)	0.036	0.007	0.005
$K_0 = 100, J_0 = 0$			
Zidi et al. [19]	1.29862	0.52553	0.30557
Present	1.29951	0.52554	0.30556
Difference(%)	0.069	0.002	0.003
$K_0 = 100, J_0 = 100$			
Zidi et al. [19]	0.20193	0.08396	0.04920
Present	0.20221	0.08398	0.04920
Difference(%)	0.139	0.024	0.000

Table 2 shows the non-dimensional deflection of FGMPo square plate (Ti-6Al-4V/ ZrO₂) resting on an

elastic foundation subjected to a sinusoidally distributed mechanical-hygro-thermal loads [19], with $a = L, R \rightarrow \infty$. The non-dimensional parameters are defined as follows:

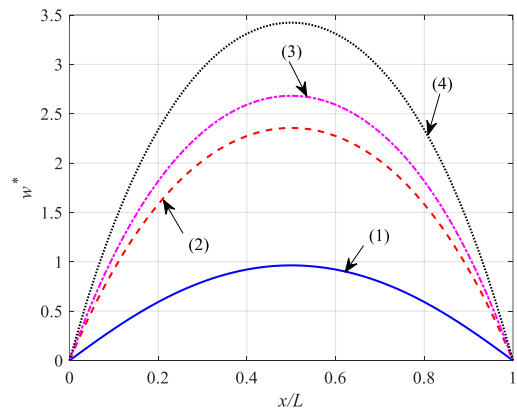
$$\hat{w} = \frac{10^2 D}{qL^4} \times w_0 \left(\frac{L}{2}, \frac{a}{2} \right); \quad D = \frac{E_c h^3}{12(1-\nu^2)} \quad (17)$$

$$K_0 = \frac{k_w L^4}{D}, J_0 = \frac{k_s L^2}{D}$$

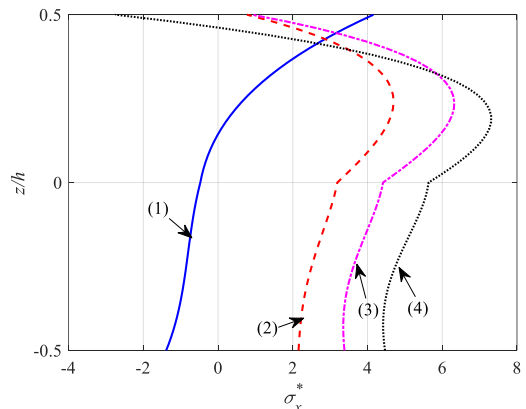
The comparison between maximum non-dimensional deflection and Navier solution obtained via FSDT with four displacement variables by Zidi et al. [19].

Table 1 and Table 2 depict the insignificant difference between this study and the precious research, thus, the analytical solution and the written Matlab code are reliable.

Unless otherwise stated, the following numerical studies apply for FGMPo (Al/Al₂O₃), with input parameters: material FGMPo - 2, $p = 2$, $\zeta = 0.15$, $h = 0.01$ m, $R/h = 100$, $L = a = 0.1 \times R$, transverse load $q = -5 \times 10^6$ Pa, temperature and moisture increase gradually $\Delta T = 50^\circ\text{C}$, $\Delta C = 0.5\%$.



(a) Variation of w^* at the cross-section $y = a/2$



(b) Variation of σ_x^* at the center of cylindrical panel

Figure 2. Variation of w^* and shear stress σ_x^* of cylindrical panel with various temperature and moisture parameters

Figure 2 shows the influence of temperature and moisture parameters on the changes in deflection and stress (w^* , σ_x^*) of the FGMPo cylindrical panel. The applied load includes mechanical load and thermal and moisture factors, varying across four cases: (1) $\Delta T = 0, \Delta C = 0$;

(2) $\Delta T = 50^\circ\text{C}$, $\Delta C = 0.5\%$; (3) $\Delta T = 100^\circ\text{C}$, $\Delta C = 0.5\%$; (4) $\Delta T = 50^\circ\text{C}$, $\Delta C = 1\%$. The graph indicates that thermal-moisture loading significantly affects the bending behavior of the cylindrical panel. In particular, the presence of thermal-moisture factors increases the maximum deflection w_{\max}^* by 2.44, 2.78 and 3.55 in cases (1), (2), (3) and (4), respectively. Additionally, hygro-thermal factors have led to the variation pattern of stress, with the positions of extreme stress points differing from those under purely mechanical loading. It is necessary to have detailed studies for each case to consider their effects.

Figure 3 illustrates the impact of the elastic foundation parameters K_0, J_0 significantly on the dimensionless deflection \bar{w} of cylindrical panel. Moreover, as the stiffness of the elastic foundation K_0, J_0 increases (with higher values of the foundation parameters), the deflection \bar{w} declines: \bar{w} decreases almost linearly with an increase in K_0 , and decreases rapidly in a nonlinear manner with an increase in J_0 .

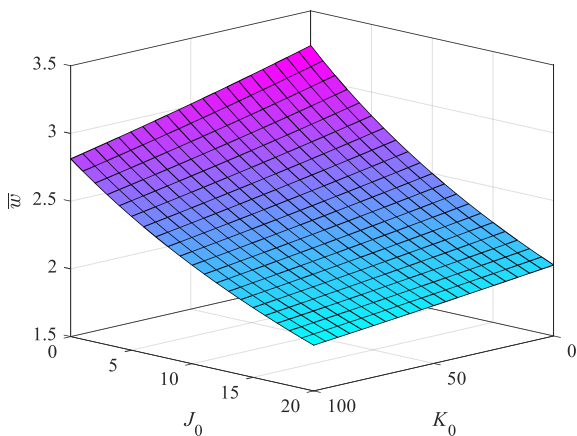
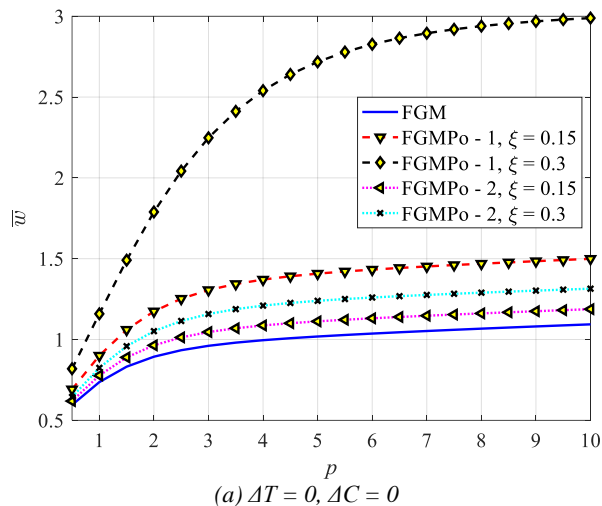


Figure 3. The effect of elastic foundation parameters K_0, J_0 on dimensionless deflection \bar{w} of cylindrical panel

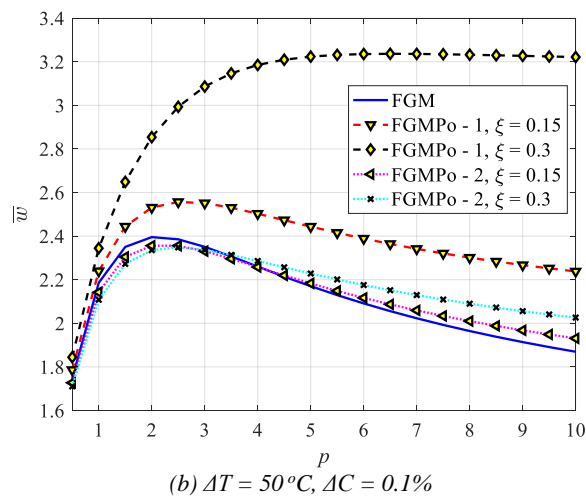
Figure 4 shows the impact of material parameters (the volume fraction index p , porosity coefficient ζ and porosity distribution types) on the dimensionless deflection \bar{w} of cylindrical panel. It can be observed that there is a clear difference when the panel is subjected only to mechanical load and when it is subjected to the combination of mechanical, thermal, and moisture load.

To be more specific that in the case of panel suffering mechanical load only (as shown in Figure 4a with different porosity distribution types and porosity coefficient ζ , when p increases (it means that the amount of ceramic falls) the deflection of cylindrical panel goes up. The perfect FGM panel has the smallest deflection, while imperfect FGM panels show larger deflections; for the same porosity coefficient ζ , FGPM-2 has a smaller deflection compared to FGPM-1. For imperfect FGM panels, as the porosity coefficient ζ increases, the stiffness of the panel decreases, leading to increased deflection. Besides, for each p , when ζ ranges from 0.1 to 0.3, the even porosity distribution has a greater increase than the uneven ones. For instance, at $p = 10$, when ζ increases from 0.1 to 0.3 FGMP-2 panel has

deflection \bar{w} grows 10.65%, whereas when FGMP-1 panel has deflection \bar{w} increases by 99.34%.



(a) $\Delta T = 0, \Delta C = 0$



(b) $\Delta T = 50^\circ\text{C}, \Delta C = 0.1\%$

Figure 4. Variation \bar{w} of cylindrical panel according to the volume fraction index p , porosity coefficient ζ and porosity distribution

In the case of panel suffering mechanical, thermal, and moisture load (as given in Figure 4b): when p changes, deflection \bar{w} has complicated variation: initially when p is small, \bar{w} goes up when p has an improvement, when p is big enough \bar{w} reaches the peak. After that, \bar{w} declines slightly while p keeps going up. The FGPM-1 distribution exhibits the highest deflection compared to the perfect FGM and FGPM-2 (with the same porosity coefficient ζ); as ζ increases, the deflection of FGPM-1 also increases. FGPM-2 and the perfect FGM panel exhibit different behaviors depending on the index p : when p is insignificant ($p \leq 2.5$), the perfect FGM has the largest deflection, and increasing the porosity coefficient ζ of FGPM-2 reduces deflection; for large ($p \geq 4.5$) the situation reverses, with the perfect FGM having the smallest deflection, and increasing the porosity coefficient ζ of FGPM-2 results in increased deflection.

Figure 5 depicts the variation of the dimensionless deflection of the cylindrical panel based on the aspect ratios a/R and R/h . It is observed that increasing the ratios

R/h (increasing radius R) or a/R (increasing side length a) both reduce the deflection. The deflection decreases rapidly when the ratios a/R and R/h have small values, and decreases more gradually when these ratios have larger values.

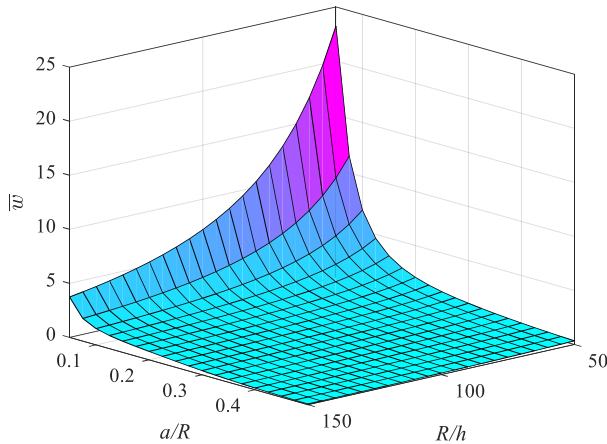


Figure 5. Variation of dimensionless deflection \bar{w} according to aspect ratios a/R , R/h

4. Conclusion

This study has established an analytical solution based on First-Order Shear Deformation Theory (FSDT), using Navier's solution form to investigate the static behavior of the FGMPo cylindrical panel. The panel is placed on a Pasternak elastic foundation, has simply supported boundary conditions along its perimeter, and is subjected to combined mechanical and hygro-thermal loading. Numerical investigations reveal the significant influence of material parameters, geometric dimensions, and the elastic foundation on the deflection and stress field of the panel. Overall, hygro-thermal factors have varying levels of impact on the static behavior of the cylindrical panel, requiring detailed analysis in each specific case.

Acknowledgments: This research is funded by the Hanoi University of Civil Engineering (HUCE) under grant number 02-2024-NNCM-DHXDHN.

REFERENCES

- [1] D. K. Jha, T. Kant, and R. K. Singh, "A critical review of recent research on functionally graded plates", *Composite structures*, vol. 96, pp. 833-849, 2013. <https://doi.org/10.1016/j.compstruct.2012.09.001>
- [2] L. W. Zhang, Z. X. Lei, K. M. Liew, and J. L. Yu, "Static and dynamic of carbon nanotube reinforced functionally graded cylindrical panels", *Composite Structures*, vol. 111, pp. 205-212, 2014. <https://doi.org/10.1016/j.compstruct.2013.12.035>
- [3] D. T. Huan, T. M. Tu, and T. H. Quoc, "Analytical solutions for bending, buckling and vibration analysis of functionally graded cylindrical panel", *Vietnam Journal of Science and Technology*, vol. 55, no. 5, pp. 587-597, 2017. <https://doi.org/10.15625/2525-2518/55/5/8843>.
- [4] J. Yang and H. -S. Shen, "Free vibration and parametric resonance of shear deformable functionally graded cylindrical panels", *Journal of Sound and Vibration*, vol. 261, no. 5, pp. 871-893, 2003. [https://doi.org/10.1016/S0022-460X\(02\)01015-5](https://doi.org/10.1016/S0022-460X(02)01015-5)
- [5] H. -S. Shen, "Postbuckling analysis of axially loaded functionally graded cylindrical panels in thermal environments", *International Journal of Solids and Structures*, vol. 39, no. 24, pp. 5991-6010, 2002. [https://doi.org/10.1016/S0020-7683\(02\)00479-1](https://doi.org/10.1016/S0020-7683(02)00479-1)
- [6] N. D. Duc and H. V. Tung, "Nonlinear response of pressure-loaded functionally graded cylindrical panels with temperature effects", *Composite Structures*, vol. 92, no. 7, pp. 1664-1672, 2010. <https://doi.org/10.1016/j.compstruct.2009.11.033>
- [7] X. Zhao, Y. Lee, and K. M. Liew, "Thermoelastic and vibration analysis of functionally graded cylindrical shells", *International Journal of Mechanical Sciences*, vol. 51, no. 9-10, pp. 694-707, 2009. <https://doi.org/10.1016/j.ijmecsci.2009.08.001>
- [8] D. Shahsavari, M. Shahsavari, L. Li, and B. Karami, "A novel quasi-3D hyperbolic theory for free vibration of FG plates with porosities resting on Winkler/Pasternak/Kerr foundation", *Aerospace Science and Technology*, vol. 72, pp. 134-149, 2018. <https://doi.org/10.1016/j.ast.2017.11.004>
- [9] Y. Q. Wang and J. W. Zu, "Vibration behaviors of functionally graded rectangular plates with porosities and moving in thermal environment", *Aerospace Science and Technology*, vol. 69, pp. 550-562, 2017. <https://doi.org/10.1016/j.ast.2017.07.023>
- [10] T. M. Tu, N. V. Long, P. T. Hang, T. V. Binh, and T. T. Hien, "Static analysis of functionally graded plates with porosities resting on Kerr's elastic foundation within the framework of simple first-order shear deformation theory", *Journal of Science and Technology in Civil Engineering (JSTCE)-HUCE*, Vietnamese version, vol. 17, no. 4V, pp. 49-63, 2023. [https://doi.org/10.31814/stce.huace2023-17\(4V\)-05](https://doi.org/10.31814/stce.huace2023-17(4V)-05)
- [11] L. T. Hai, N. V. Long, and T. M. Tu, "Free vibration and dynamic response of functionally graded plates with porosities resting on Kerr's elastic foundation", *Journal of Science and Technology in Civil Engineering (JSTCE)-HUCE*, Vietnamese version, vol. 18, no. 3V, pp. 1-15, 2024. [https://doi.org/10.31814/stce.huace2024-18\(3V\)-01](https://doi.org/10.31814/stce.huace2024-18(3V)-01)
- [12] N. Wattanasakulpong and V. Ungbhakorn, "Linear and nonlinear vibration analysis of elastically restrained ends FGM beams with porosities", *Aerospace Science and Technology*, vol. 32, no. 1, pp. 111-120, 2014. <https://doi.org/10.1016/j.ast.2013.12.002>
- [13] N. Wattanasakulpong, B. G. Prusty, D. W. Kelly and M. Hoffman, "Free vibration analysis of layered functionally graded beams with experimental validation", *Materials & Design (1980-2015)*, vol. 36, pp. 182-190, 2012. <https://doi.org/10.1016/j.matdes.2011.10.049>
- [14] J. N. Reddy, *Mechanics of laminated composite plates and shells: theory and analysis, second edition*. CRC press, 2003.
- [15] A. M. Zenkour, "The refined sinusoidal theory for FGM plates on elastic foundations", *International journal of mechanical sciences*, vol. 51, no. 11-12, pp. 869-880, 2009. <https://doi.org/10.1016/j.ijmecsci.2009.09.026>
- [16] Z. Huang, C. Lü, and W. Chen, "Benchmark solutions for functionally graded thick plates resting on Winkler-Pasternak elastic foundations", *Composite Structures*, vol. 85, no. 2, pp. 95-104, 2008. <https://doi.org/10.1016/j.compstruct.2007.10.010>
- [17] M. Sobhy, "An accurate shear deformation theory for vibration and buckling of FGM sandwich plates in hygrothermal environment", *International Journal of Mechanical Sciences*, vol. 110, pp. 62-77, 2016. <https://doi.org/10.1016/j.ijmecsci.2016.03.003>
- [18] H. -T. Thai and D. -H. Choi, "A refined plate theory for functionally graded plates resting on elastic foundation". *Composites Science and Technology*, vol. 71, no. 16, pp. 1850-1858, 2011. <https://doi.org/10.1016/j.compotech.2011.08.016>
- [19] M. Zidi, A. Tounsi, M. S. A. Houari, and O. A. Bég, "Bending analysis of FGM plates under hygro-thermo-mechanical loading using a four variable refined plate theory", *Aerospace Science and Technology*, vol. 34, pp. 24-34, 2014. <https://doi.org/10.1016/j.ast.2014.02.001>